Pharm Res (2015) 32:1604–1614
DOI 10.1007/s11095-014-1560-7

RESEARCH PAPER

Thermosensitive Liposome Formulated Indocyanine Green for Near-Infrared Triggered Photodynamic Therapy: *In Vivo* Evaluation for Triple-Negative Breast Cancer

Colby S. Shemesh • Delaram Moshkelani • Hailing Zhang

Received: 28 July 2014 / Accepted: 27 October 2014 / Published online: 19 November 2014

ABSTRACT

Purpose The focus of this research was to formulate and evaluate a theranostic liposomal delivery system using indocyanine green (ICG) as a photosensitizer, triggered by near infrared (NIR) irradiation, for *in vivo* photodynamic therapy (PDT) of breast cancer.

Methods Cytotoxicity of PDT using liposomal ICG (LPICG) as well as free ICG (FRICG) was evaluated in the human MDA-MB-468 triple-negative breast cancer (TNBC) cell line. NIR irradiation-induced increase in temperature was also monitored both *in vitro* and *in vivo*. Quantitative pharmacokinetic profile and fluorescence imaging-based biodistribution patterns of both formulations were obtained using the human TNBC xenograft model in nude mice. Overall safety, tolerability, and long-term anti-tumor efficacy of LPICG *versus* FRICG-mediated PDT was evaluated.

Results Significant loss of cell viability was achieved following photoactivation of LPICG *via* NIR irradiation. Temperatures of irradiated LPICG increased with increasing concentrations of loaded ICG, which correlated with significant rise of temperature compared to PBS *in vivo* ($p < 0.01$). Pharmacokinetic assessment revealed a significant increase in systemic distribution and circulation half-life of LPICG, and NIR fluorescence imaging demonstrated enhanced accumulation of liposomes within the tumor region. Tumor growth in mice treated with LPICG followed by NIR irradiation was significantly reduced compared to those treated with FRICG, saline, and irradiation alone.

Conclusions *In vivo* photodynamic therapy using LPICG demonstrated targeted biodistribution and superior anti-tumor efficacy in a human TNBC xenograft model compared to FRICG. In addition, this unique delivery system exhibited a promising role in NIR image-guided delivery and real-time biodistribution monitoring of formulation with ICG serving as the fluorescent probe.

C. S. Shemesh • D. Moshkelani • H. Zhang (✉)
Drug Delivery Laboratory, Department of Pharmaceutical Sciences
College of Pharmacy, Mercer University, 3001 Mercer University Drive
Atlanta, Georgia 30341, USA
e-mail: Hailing.Zhang@fda.hhs.gov

KEY WORDS indocyanine green · liposomes · near-infrared florescence imaging · photodynamic therapy · triple-negative breast cancer

ABBREVIATIONS

EPR	Enhanced permeation and retention
FRICG	Free indocyanine green
LPICG	Liposomal indocyanine green
NIR	Near-infrared
PDT	Photodynamic therapy
PEG	Polyethylene Glycol
ROS	Reactive oxygen species
TNBC	Triple-negative breast cancer

INTRODUCTION

Substantial advancements in the area of cancer research within the past decade have led to emergence of several novel therapeutic approaches besides the mainstream surgical resection, radiation therapy, and chemotherapy. Photodynamic therapy (PDT) is among these alternative and modern modalities, which has recently garnered increasing attention for applications in oncology due to its selectivity, minimal systemic toxicity, and non-invasive features (1–3). This light-based approach was approved approximately two decades ago by the Food and Drug Administration as the first drug-device combination, yet currently oncological applications of PDT are far under utilized (4). Due to the negligible side effects of PDT, sparing of organ function, and excellent compatibility with current therapeutic modalities such as chemo/radio therapy, there is a convincing demand for the revival of this promising treatment modality.

Photodynamic therapy involves the use of a biocompatible photosensitizer and light energy of optimal wavelength to initiate photochemical reactions. The cytotoxic effects of

PDT are based on the generation of reactive oxygen species (ROS), which stem from both *type I* (direct substrate interaction with radical formation) and *type II* (direct energy transfer to molecular oxygen) reactions (5). These ROS induce oxidative damage to bioorganic molecules including proteins, nucleic acids, carbohydrates, and lipids, consequently leading to destruction and death of targeted cancer cells. PDT has been used in the clinic with high efficacy for a wide variety of oncological applications including treating cancers of the brain, head and neck, lung, breast, pancreas, intraperitoneal cavity, colon, prostate, and skin (1,6).

More recently, an increasing amount of research has been conducted in evaluating and improving photosensitizers to enhance the efficacy of PDT in various cancer types (7–14). Our particular photosensitizer of interest is indocyanine green (ICG), which is a water-soluble, anionic tricarbocyanine dye commonly used in numerous medical imaging and diagnostic applications (15). ICG is very safe and well tolerated, with a high lethal dose (LD_{50}) between 50 and 80 mg/kg in animals (16). As a non-toxic organic near-infrared (NIR) dye ICG is also an attractive photosensitizer for PDT due to its strong absorption at 805 nm with minimal bioscattering and limited autofluorescence of biomolecules at this wavelength. Consequently, deeper tissue penetration and higher signal-to-noise ratio images can be achieved using ICG as opposed to other photosensitizers excited at shorter wavelengths (17,18).

Despite its many positive attributes, ICG exhibits poor pharmacokinetics and limited *in vivo* photostability when used in its free solution form for PDT (19,20). Nanotechnology may be employed to enhance the formulation properties and thereby improve its efficacy in PDT by offering protection against aqueous degradation and prolonging circulation half-life (21–24). As a modern emerging platform for cancer therapy, nanotechnology involves the use of nano-sized drug carriers smaller than 100 nm in diameter to offer enhanced delivery of drugs. It is well established that the tumorous region tends to undergo fast blood vessel production due to increased demands of the rapidly proliferating cells for oxygen and nutrients. Consequently, abnormalities in the fluid transport and lymphatic system in addition to formation of poorly aligned endothelial cells and wide fenestrations cause nanoparticles to be preferentially accumulated and retained in the tumor site known as the enhanced permeation and retention effect (EPR) (25). Liposomes are among one of many nanocarrier systems and are distinguished by having a closed colloidal structure composed of self-assembling lipid bilayers, which allow the encapsulation of hydrophilic as well as incorporation of lipophilic molecules. Furthermore, surface conjugation of polymers such as polyethylene glycol (PEG) affords reduced clearance and longer half-life of the vesicle *via* limited detection and degradation by cells of the immune system (26).

Previously, a thermosensitive liposomal formulation of ICG (LPICG) was developed and evaluated in our laboratory which exhibited excellent stability at 37°C, yet a gel to liquid transition and burst release effect at temperatures above 42°C was obtained (27). Furthermore, LPICG-based PDT was extensively investigated in our most recent publication, which demonstrates a comprehensive *in vitro* evaluation and optimization of this approach for treatment of triple-negative breast cancer (TNBC) cells (28). TNBC is considered to be one of the most aggressive and least responsive forms of breast cancer due to absence of cell surface receptors that can serve as targets for small molecule and or hormonal therapeutics (29). Furthermore, genomic alternations associated with TNBC has shown to render the cells particularly more sensitive to oxidative damage (30). Subsequently, lack of effective and targeted therapy calls for development of alternative therapeutic strategies such as PDT. The results from our previous study illustrated a significant *in vitro* cytotoxic potential across a panel of TNBC cells (28). Due to these promising outcomes, we sought to evaluate this liposomal delivery system for PDT *in vivo* anticipating enhanced pharmacokinetics and biodistribution of LPICG leading to improved and localized destruction of the cancer tissue. Accordingly, the most responsive TNBC cell line, MDA-MB-468, was selected for this work to establish a xenograft model in nude mice and conduct the proposed *in vivo* studies for illustration of enhanced and localized PDT for the tumor.

MATERIALS AND METHODS

Materials

Heparinized mouse plasma was purchased from Innovative Research (Novi, MI). Isoflurane for anesthesia was purchased from Butler Schein Animal Health (Dublin, OH). Matrigel was purchased from BD Biosciences Inc. (San Diego, CA). 1, 2-dipalmitoyl-sn-glycero-3-phosphocholine (DPPC) and L-α-phosphatidylcholine (Soy-PC) were purchased from Avanti Polar Lipids (Alabaster, AL). N-(carbonyl-methoxypolyethyleneglycol 2000)-1, 2-distearoyl-sn-glycero-3-phosphoethanolamine ($DSPE–PEG_{2000}$) was purchased from NOF Corporation (Tokyo, Japan). Cholesterol was purchased from Alfa Aesar (Ward Hill, MA). Indocyanine green, IR-820, dimethylsulfoxide (DMSO >99.9% reagent grade), formic acid, MTT, ammonium acetate and Sephadex G-75 were obtained from Sigma-Aldrich (St. Louis, MO). Acetonitrile and fetal bovine serum were acquired from Fisher Scientific (Hanover Park, IL). DMEM and phosphate buffered saline were purchased from Life Technologies (Grand Island, NY). Penicillin streptomycin (PS) was purchased from Atlanta Biologicals (Lawrenceville, GA). Aminopropyl columns (20 mg, 1 cc, CEREX) were purchased from SPEware Corporation (Baldwin Park, CA). Infrared

thermometer and thermocouple probe were obtained from Fisher Scientific (Hanover Park, IL).

Preparation and Characterization of Liposomal ICG (LPICG)

LPICG was formulated *via* a standard thin film/extrusion method, with a formulation composition of DPPC: Soy-PC: Chol: DSPE-PEG_{2000} in a molar ratio of 100:50:30:0.5. The total mass of lipids used was 20 mg. Formulation components were placed into a 25-mL round-bottom flask with the addition of 1–2 mL of chloroform/methanol (2:1) solution to dissolve the lipids. The solvent was then rotoevaporated at 37°C to yield a thin film followed by overnight vacuum to remove any residual solvent. The next day, an aqueous solution of ICG was prepared at a concentration of 10 mg/mL and used to hydrate the film at 60°C for 1 h to form multilamellar liposome vesicles. Following hydration, the liposomal suspension was passed through a mini-extruder set, with 100-nm polycarbonate membrane, 19 times at 65°C to generate uni-lamellar liposomes. Unencapsulated ICG was isolated from the liposomal suspension *via* size exclusion chromatography using Sephadex G-75. The particle size distribution of liposomes was measured using Malvern Nano Zetasizer (Worcestershire, United Kingdom). ICG was quantified by high-pressure liquid chromatography-electrospray ionization tandem mass spectrometry (HPLC-ESI-MS-MS) using an Agilent 1200 series HPLC coupled to an Agilent 6410B QQQ mass spectrometer (Agilent, Santa Clara, CA) with IR-820 as the internal standard. Chromatographic separation was achieved using an Agilent Zorbax Eclipse Plus (100 mm × 2.1 mm, 3.5 μm) C18 column with the column compartment maintained at 35°C using an injection volume of 15 μL. A gradient elution was used with elution solvents composed of 10 mM ammonium acetate solution at pH 3.0, adjusted by formic acid (A) and acetonitrile (B) according to the following gradient: 0–2.5 min (45% B), 2.5–3.0 min (75% B), 3.01–7.0 min (75% B), and 7.0–7.01 min (45% B) with a 4.5-min post-run using a constant flow rate of 0.45 mL/min. The retention times for ICG and IR-820 were 2.7 and 6.2 min, respectively. Positive mode ionization conditions were optimized using a (N_2) drying gas temperature set to 350°C, flow rate of 12 L/min, nebulizer spray at 35 psi, and capillary voltage of 3,000 V. Multiple reaction monitoring (MRM) mode was used with a corresponding dwell time set to 100 msec and an electron multiplier voltage setting of + 400 V. For ICG, an SRM transition of (m/z 753→330 Da) was used as the quantifier and (827→330 Da) for IR-820, using a fragmentor voltage of 160 V and collision energy of 38 V to monitor both. All of the formulations in this study were used within less than 24 h to avoid and/or minimize aggregation, quenching, and degradation of ICG.

Cell Culture

Human TNBC cell line MDA-MB-468 was provided by Dr. Ruth O'Regan from Winship Cancer Institute, Emory University School of Medicine. MDA-MB-468 cells were grown in DMEM supplemented with 100 units/mL of penicillin and 100 μg/mL streptomycin in addition to 10% fetal bovine serum, in a humidified incubator set at 37°C with 5% CO_2. Growth media was replaced every three days and cellular confluence and morphology were periodically monitored.

Cytotoxicity Assessment of PDT Across Pig Ear Skin

Sections of isolated pig ear skin were used to evaluate the penetration depth of NIR irradiation and evaluate the cytotoxic effects of NIR-induced PDT across the tissue. The thickness of pig ear skin was measured to be approximately 1.75 mm using a vernier caliper with an average area of 8.0 cm^2. Briefly, MDA-MB-468 cells were seeded at 50,000 cells in 35 × 10 mm culture plates and placed in a humidified incubator maintained at 37°C with 5% CO_2 overnight. The next day, cells were rinsed with PBS and replaced with 37.5 μM solution of LPICG followed by incubation for 10 h to obtain internalization of the photosensitizer. LPICG was then removed and cells were thoroughly rinsed with 1 mL of PBS. Next, a section of pig ear skin tissue was placed directly over each petri dish to cover the cells entirely and the plate was irradiated using a 2-W, 0.5-m NIR fiber-coupled laser diode consisting of bundle diameter of 6.2 mm and individual fiber diameter of 100 μm (Edmund Optics, Barrington, NJ). The laser system was calibrated in milliwatts (mW) and LD milliamp current (mA) with a maximal energy output of 2 W emitting at 808 nm, using laser fluences of 0, 15, 30, 60, and 100 J/cm^2. Following light exposure, PBS was immediately removed and replaced with fresh growth media incubated for another 24 h after which cytotoxicity was determined *via* MTT assay. Briefly, 10 μL of 3-(4, 5-dimethylthiazol)-2, 5-diphenyltetrazolium bromide (MTT) solution in PBS (5 mg/mL) was added to cells and incubated for approximately 3 h at 37°C. The media were then removed, the resulting formazan crystals were dissolved in 100 μL of DMSO, and absorbance was measured at 570 nm using a Synergy HT plate reader (Bio-Tek Instruments, Winooski, VT). Cell viability was determined by taking the signal from treated groups over control groups without irradiation. All experiments were carried out in triplicates and data was plotted as the mean values ± standard deviation (SD).

Tumor Xenograft Murine Model

Female athymic nude mice (*nu/nu*, 4–6 weeks old weighing 18–22 g) were purchased from Charles River Laboratories (Wilmington, MA) and animals were received and cared for

according to the protocols approved by the Institutional Animal Care and Use Committee of Mercer University (IUCAC Approval Number: A1307009). Animals were housed in autoclaved cages and maintained under a 12-h light/dark cycle at temperatures ranging form 20–25°C, with continuous access to food and water *ad libitum*. Mice were initially quarantined and acclimatized for 1 week following arrival. Tumor growth was induced by subcutaneous implantation of human TNBC MDA-MB-468 cells (4×10^6 in a 0.1 mL matrigel/DMEM mixture) on the right and left lower flanks of the mice (31,32). Tumor-bearing animals were then allowed to reach mean tumor volumes of 50–100 mm^3 followed by randomization of the mice into appropriate treatment and controls groups. Visible tumor masses usually appeared roughly 10 days after implantation. Tumor volumes and total body weight were recorded routinely. The tumor volumes were measured using a caliper and calculated as $(width)^2\times$ length/2, where width was measured as the shortest diameter and length as the longest diameter of the nodules.

Quantitative Pharmacokinetic Evaluation of FRICG and LPICG

After mean tumor volumes reached between 50 and 100 mm^3, animals were randomized into groups consisting of 4 mice per group to determine the whole body disposition of free ICG (FRICG) and LPICG. Mice were fasted overnight (~8 h) with *ad libitum* water, weighed the next morning, and administered intravenously with diluted FRICG or LPICG in PBS at 5 mg/kg, *via* the tail vein. Staggered sampling was performed *via* retro-orbital whole blood collection at 0, 5, 15, 30, 60, 120, and 180 mins following injection. Protein precipitation using a novel anion exchange solid phase extraction methodology was employed to separate and purify ICG from plasma, which was isolated from whole blood by centrifugation at 2,500 g for 10 mins at 20°C. 50 μL of each plasma fraction was then transferred into a separate tube with the addition of internal standard to each sample at 500 ng/mL. Protein precipitation was performed using 100 μL of cold acetonitrile, whereby samples were vortexed for 0.5 mins and centrifuged at 10,000 g for 5 mins. Aminopropyl columns (20 mg, 1 mL, CEREX) were conditioned using 500 μL of methanol, followed by charging the sorbent using 500 μL of acetate buffer (100 mM, pH 4.5). Samples were then applied onto the sorbent and rinsed with 500 μL of water followed by 500 μL of methanol, and allowed to dry under vacuum for 10 mins. Rinse tubes were replaced with sample collection tubes and ICG was eluted using two sequential 500-μL portions of 2% NH_4OH in MeOH. Samples were then evaporated to dryness followed by reconstitution in 100 μL of mobile phase and transferred into autosampler vials for HPLC-ESI-MS-MS analysis as described in the previous section. Pharmacokinetic parameters were calculated by non-compartmental analysis using the Phoenix WinNonlin v 6.3 software (Pharsight, Sunnyvale, CA).

In Vivo NIR Fluorescence Imaging and Terminal Biodistribution Assessment

Once the tumor volumes reached an average of 400–500 mm^3, mice were randomized into two groups injected with either FRICG or LPICG at ICG dose of 5 mg/kg. Formulations were administered intravenously *via* the tail vein and whole body imaging was performed using the Odyssey bioimaging system (LI-COR Biosciences, Lincoln, NE) at 0, 4, 8, 24, and 48 h after dosing. The average fluorescence intensity corresponding to tumors on each side was calculated and compared between FRICG and LPICG groups. For determination of terminal biodistribution of both FRICG and LPICG, Mice were intravenously injected with 5 mg/kg of each formulation, sacrificed 24 h later, and organs including the heart, lung, liver, spleen, kidneys as well as the tumor were excised, weighed, and imaged *via* the Odyssey bioimager using 800 nm as the fluorescence spectral channel. The mean fluorescent intensity signal for each organ was integrated and compared between the two treatment groups ($n=3$).

NIR Irradiation-Induced Temperature Effects

Temperature effects during NIR irradiation were evaluated *in vitro* using concentrations of LPICG equivalent to 6, 12, and 24 μg/mL in comparison to a blank PBS solution. Temperatures were monitored using a thermocouple probe with measurements made every 30 s for a total of 5 mins during exposure of LPICG and PBS solutions to 2 W/cm^2 of NIR irradiation. Additionally, irradiation-induced temperature effects were evaluated *in vivo* using the tumor-bearing mice injected with PBS, FRICG, or LPICG (5 mg/kg ICG dose) and irradiated after 6 h. The maximal irradiation output energy was adjusted to 2 W/cm^2 corresponding to 2 mins of light exposure and total fluence of 240 J/cm^2. Irradiation-induced temperature increases for both treatment and control groups were recorded using a thermocouple probe placed at the tumor flank with measurements made every 10 s during the 2-min irradiation period.

In Vivo Anti-Tumor Efficacy of LPICG-Mediated PDT

When nude mice inoculated with MDA-MB-468 cells on lower flanks reached an average tumor volume of 50–75 mm^3 mice were randomized into five groups consisting of PBS alone, PBS + laser, LPICG alone, LPICG + laser, and FRICG + laser. Mice were weighed and administered with either 200 μL of PBS, 5 mg/kg FRICG, or 5 mg/kg LPICG followed by localized NIR irradiation of the tumor site 6 h later for 2 mins at 2 W/cm^2. Mice were weighed and tumor

sizes were measured every 3 to 4 days with volumes calculated as $(\text{width})^2 \times \text{length}/2$.

Statistical Analysis

Statistically significant differences between groups were evaluated using analysis of variance (ANOVA) and Student's *t*-test. All experiments were carried out in triplicates ($n=3$) and mean values with standard deviation (SD) were used to plot the figures. P values <0.05 were considered to be statistically significant.

RESULTS AND DISCUSSION

Preparation and Characterization of LPICG

The mean hydrodynamic diameter of LPICG was 79.8± 11.6 nm (Fig. 1a). After size exclusion chromatography, liposomes were routinely quantified using a newly developed and validated assay for reversed phase HPLC coupled to electrospray ionization tandem mass spectrometry. Liposomes hydrated with appropriate concentration of ICG (~8–10 mg/mL) and yielded encapsulated ICG levels between 500 and 700 μg/mL after purification, which were subsequently diluted in PBS. A representative chromatogram is provided in Fig. 1b, which illustrates the chromatographic separation and subsequent mass spectroscopy analysis of ICG using IR-820 as an internal standard.

Cytotoxicity Assessment PDT Across the Pig Ear Skin

In an attempt to demonstrate the effective laser light depth of penetration in the NIR region leading to cytotoxic effects, LPICG-mediated PDT of MDA-MB-468 cells were achieved by irradiation across pig ear skin. As described earlier, combination of ICG with NIR laser irradiation results in excitation of the photosensitizer that induces the photooxidative and subsequent cytotoxic effects of PDT on cancer cells (31–33). The induction of DNA and protein damage mediated by generation of ROS in this process has been well established and characterized in the literature (34). Furthermore, liposomal encapsulation of photosensitizers other than ICG have been attempted and evaluated *in vitro and ex vivo* by other researchers for cancer treatment, which have shown to be very beneficial (35). We expect that liposomal ICG will be excited by NIR irradiation and anticipate that excited ICG molecules are released due to increase in temperature, which in turn will react with the surrounding oxygen. Additionally, laser light can readily penetrate through the liposomal bilayer to activate the ICG molecules to generate ROS, which may freely diffuse across the bilayer. As observed in Fig. 2, the photodynamic effect is evident in a directly proportional dose–response pattern with greater cell death observed at increasing laser light fluences ranging from 0 to 100 J/cm^2. Furthermore it is shown that the laser light is readily capable

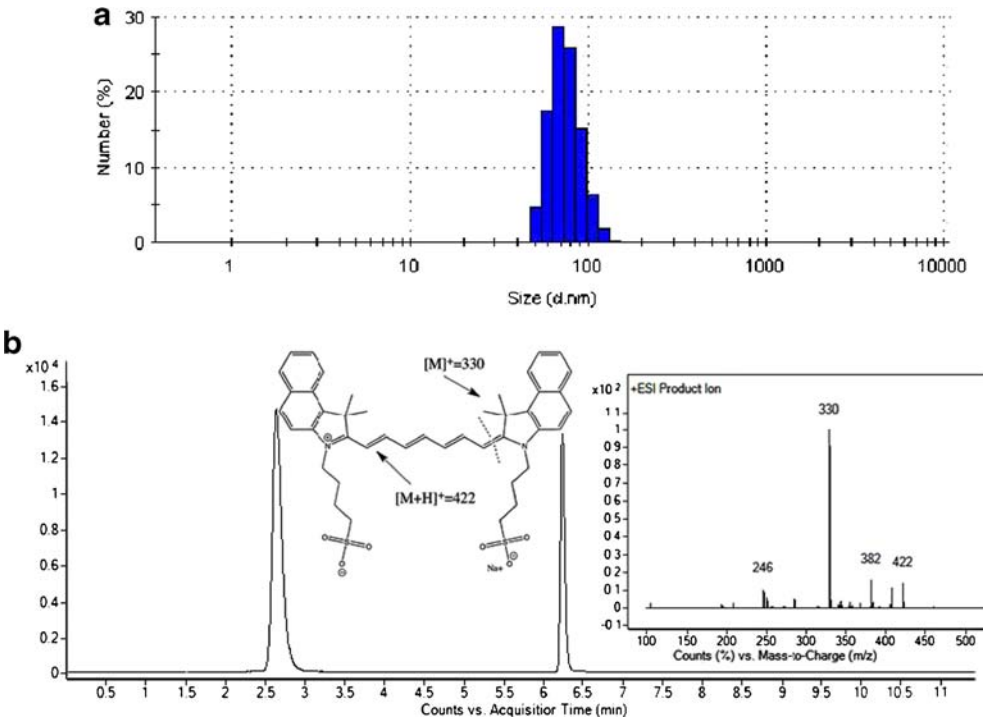

Fig. 1 (**a**) An illustrative size distribution plot for ICG-loaded liposomes with mean hydrodynamic diameter of 79.8 ± 11.64 ($n=4$), as determined by dynamic light scattering. (**b**) Representative chromatogram of ICG and IR-820 with retention times of 2.7 and 6.2 min, respectively. Molecular structure and fragmentation pattern of ICG is shown with product ion fragmentation of 753 Da precursor. Product ion scan of m/z 753 Da is observed with high abundance ions including 330 and 422 Da. MRM for ICG and IR-820 was set up using transition ions of m/z 753→330 and 827→330 Da, respectively.

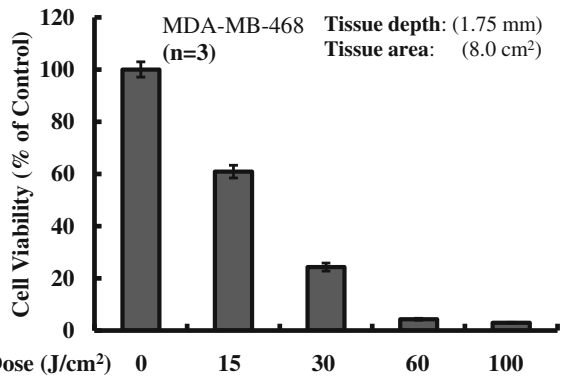

Fig. 2 Cytotoxicity profile of MDA-MB-468 cells incubated with LPICG for 10 h prior to NIR irradiation across pig ear skin with 1.75 mm thickness, using laser fluences ranging from 0 to 100 J/cm^2. Cytotoxicity was examined 24 h after illumination *via* MTT assay. Plotted values represent the mean % cell viability ± SD ($n = 3$).

of penetrating through a 1.75 mm thick pig ear skin tissue composed of a total area of 8.0 cm^2. Cytotoxicity evaluated 24 h after PDT indicated that LPICG combined with laser irradiation caused a mean 96% loss of total cell viability after a brief 4-min illumination. Hence, PDT triggered by NIR irradiation of liposomal ICG is a promising approach to be evaluated *in vivo* for its potential in treatment of cancer.

Quantitative Pharmacokinetic Evaluation of FRICG and LPICG

Nano-based drug delivery using liposome carrier systems have been demonstrated to enhance the pharmacokinetic profile due to EPR effect and ultimately depend on the bio-physical properties of the formulation such as size, charge, and PEGylation (36). Using a novel extraction and analytical assay for ICG with a limit of quantitation at 10 ng/mL, adequate sensitivity and specificity were obtained to allow characterization of FRICG and LPICG plasma concentrations over time following i.v. bolus dosing of tumor-bearing athymic mice. The method was demonstrated to have an excellent extraction efficiency with recoveries >95% for ICG, which is a critical feature for assaying samples with limited volume. Non-compartmental modeling using WinNonlin was performed with plasma concentration time profiles evaluated for FRICG and LPICG demonstrating the whole body disposition of ICG (Fig. 3). Pharmacokinetic estimations for both formulations are summarized in Table I.

Immediately 5 min after dosing, the mean maximum concentrations (C_{max}) in plasma were 1573.1±429.0 and 10099.2± 1627.2 ng/mL for FRICG and LPICG, respectively ($p < 0.01$). LPICG exhibited over a 6-fold increase in ICG plasma concentrations. The mean area under the plasma concentration time curve from zero to infinity ($AUC_{0-\infty}$) was determined to be 611.2 ±176.4 ng.hr/mL for FRICG *versus* 1905.7±56.9 ng.hr/mL for LPICG ($p < 0.001$). LPICG was found to have a 3-fold higher AUC, an important metric parameter for evaluation of total

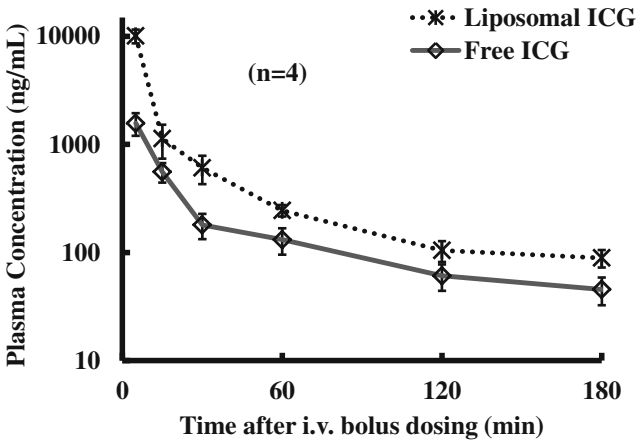

Fig. 3 ICG plasma concentration time profile following i.v. dosing using 5 mg/kg of either FRICG (*solid-line*) or LPICG (*dashed-line*) in tumor-bearing nude mice. Retro-orbital blood collection was performed at 0, 5, 15, 30, 60, 120, and 180 min after dosing. The data represent the mean plasma concentrations ± SD ($n = 4$) using staggered sampling from mice in three groups.

systemic ICG exposure. Total clearance (CL_T) and volume of distribution at steady state (V_{DSS}) were determined to be 6405.6 ±434.8 mL/hr/kg and 10830.3±2305.4 mL/kg for FRICG, and 2632.8±76.0 mL/hr/kg and 2512.2±570.6 mL/kg for LPICG, respectively ($p < 0.001$ for CL_T and $p < 0.05$ for V_{DSS}). CL_T was decreased by 3-fold using LPICG as compared to FRICG. Following i.v. bolus administration of 5 mg/kg FRICG or LPICG, the plasma concentration time profile for both decreased rapidly for the first 15 mins and then exhibited a steady elimination profile with $t_{1/2}$ of 71.3±7.8 and 82.2±10.4 mins for FRICG and LPICG, respectively. The elimination half-life was slightly extended using LPICG but was very similar to FRICG with no statistically significant difference. It was also observed that LPICG exhibited confinement to the central compartment, which is most likely attributed to the larger size of liposomal carriers (<100 nm). Results from this study are highly comparable to data in the existing literature. For instance, encapsulation of ICG in other types of nanocarriers has shown to enhance its

Table I Estimated Pharmacokinetic Parameters for Total Systemic Exposure of FRICG and LPICG in Tumor-Bearing Nude Mice ($n = 4$)

Parameter	FRICG (mean ± SD)	LPICG (mean ± SD)
$t_{1/2}$ (min)	71.3±7.8	82.2±10.4
C_{max} (ng/mL)	1573.1±429.0	10099.2±1627.2 (**)
$AUC_{0-\infty}$ (ng.hr/mL)	611.2±176.4	1905.7±56.9 (***)
CL_T (mL/hr/kg)	6405.6±434.8	2632.8±76.0 (***)
V_{DSS} (mL/kg)	10830.3±2305.4	2512.2±570.6 (*)

Abbreviations $t_{1/2}$: elimination half-life; C_{max}: maximal plasma concentration; $AUC_{0-\infty}$: area under the curve for plasma concentration time values from zero to infinity; CL_T: total clearance; V_{DSS}: estimated central compartment volume of distribution at steady state. Significant difference is shown as $p < 0.001$ (***), $p < 0.01$ (**), and $p < 0.05$ (*)

pharmacokinetic and biodistribution profiles relative to free ICG corresponding to higher accumulation of the dye in organs as well as up to 10-fold greater plasma levels following i.v. dosing (37). The pharmacokinetic analysis of this study demonstrates an approximately 6-fold increase in plasma levels as compared to FRICG after i.v. bolus dosing of LPICG.

In Vivo NIR Fluorescence Imaging and Terminal Biodistribution Assessment

Accumulation of photosensitizer within the tumor is imperative in successfully achieving the desired cytotoxic effects of PDT. Fluorescence imaging and *ex vivo* analysis of isolated organs may be readily performed in order to determine the terminal biodistribution profiles (38). A non-invasive NIR imaging approach was chosen to evaluate the accumulation, circulation, and disposition of ICG in tumor-bearing mice. Due to encapsulation of ICG in liposomes, stability of the fluorophore is largely enhanced, which in turn allows for real-time, image-guided delivery and monitoring of the formulation. Mice were pre-imaged and subsequently dosed with 5 mg/kg of either FRICG or LPICG followed by whole body scanning at various time-points including 4, 8, 24, and 48 h. It was observed that FRICG was rapidly eliminated from circulation after approximately 4 h, with only minimal residual fluorescence intensity after 8 h and nearly complete elimination after 24 h (Fig. 4a). In contrast, LPICG exhibited preferential and higher accumulation corresponding to elevated fluorescence signal within the tumor tissue up to 48 h as illustrated in Fig. 4b. Fluorescence intensity counts at the tumor site for LPICG group were also much higher as compared to FRICG and were found to be statistically significant at 4, 8, 24, and 48 h with p values <0.05, 0.05, 0.05, and 0.01, respectively (Fig. 4c). Once again, these results are consistent with the hypothesized EPR effect of nanocarriers within the tumor region due to anatomical deformities and physiological dysfunctions.

Terminal biodistribution was also assessed after administration of 5 mg/kg FRICG or LPICG and excision of organs 24 h later. It was observed that qualitatively, ICG fluorescence intensity in all organs including the tumor, heart, liver, spleen, and kidneys, with the exception of lungs, was much higher for the LPICG group (Fig. 4b). Similarly, Fig. 4d indicates that the average fluorescence intensity counts of organs including the tumor were significantly higher for LPICG than FRICG with p <0.01. These results collectively demonstrate the advantages offered by formulating LPICG including greater ICG stability, enhanced biodistribution of liposomes and accumulation at the tumor site, and reduced clearance of the formulation compared to FRICG.

NIR Irradiation-Induced Temperature Effects

Temperature effects induced by NIR irradiation were first evaluated *in vitro* using aqueous solutions containing increasing concentrations of LPICG compared to PBS solution as the control. As temperature change was monitored during laser exposure, the PBS control solution showed to have an initial temperatre spike of 5°C and stabilized to reach a maximal temperature of 30°C over 5 min of irradiation. On the other hand, a directly proportional dose–response increase was observed for LPICG with increasing loaded concentrations of ICG from 6 to 24 μg/mL corresponding to maximal temperatures of 43 to 62°C respectively. The 24 μg/mL concentration of LPICG combined with laser irradiation was found to be highly statistically significant compared to PBS plus laser with p <0.001 (Fig. 5a). Since ICG is capable of offering selective photothermal destruction of cancer cells, we next sought to evaluate the *in vivo* temperature effects (39). *In vivo* NIR-induced temperature changes during photodynamic treatment to tumored mice were examined after administration of PBS, FRICG, or LPICG at 5 mg/kg and irradiation for 2 min, 6 h after dosing using an 808 nm laser at 2.0 W/cm^2. The temperature of tumor mass in mice dosed with PBS had an average initial increase of 7°C ultimately reaching 44°C. However, the tumor mass temperature in mice administered with FRICG and LPICG exhibited increases of 8 and 10°C, respectively, with both reaching maximal temperatures close to 50°C (Fig. 5b). It is evident that mice dosed with LPICG or FEICG demonstrated the greatest rise in temperature with a signficant difference compared to PBS (p<0.01). In our previous article we performed extensive *in vitro* studies to establish the photodynamic effects of ICG triggered by NIR irradiation (28). However, heating >50°C usually has some degree of photothermal effects as well, which is directly correlated to exposition time (seconds) and density of power (w/cm^2). We expect that the majority of anti-tumor effect from our treatment is attributed to the photodynamic reaction due to our brief exposure time and overall irradiation energy in addition to the high photosensitizer concentration; that being said, using longer exposure times may augment photothermal effects. Nevertheless, given the potential photothermal capabilities of ICG and preferential accumulation in the tumor, additional localized destruction of tumor cells may be achieved to further enhance the anti-tumor efficacy of PDT (40,41). Literature has shown that tumor-bearing mice administered with ICG and stimulated by NIR laser light at 808 nm exhibited significant tissue necrosis upon histological evaluation, which gradually led to reduction of tumor volume when compared to control groups (42). Hence, LPICG delivery system irradiated by NIR laser light may even be able to achieve selective and targeted dual cytotoxic effects at the tumor site elicited *via* both PDT and photothermal therapy.

In Vivo Anti-Tumor Efficacy of LPICG-Mediated PDT

PDT has been shown to have numerous clinical applications including treatment of various cancer types by offering selectivity and high tolerability (12). Encouraged by our preliminary results using LPICG-based PDT *in vitro,* we pursued the evaluation of

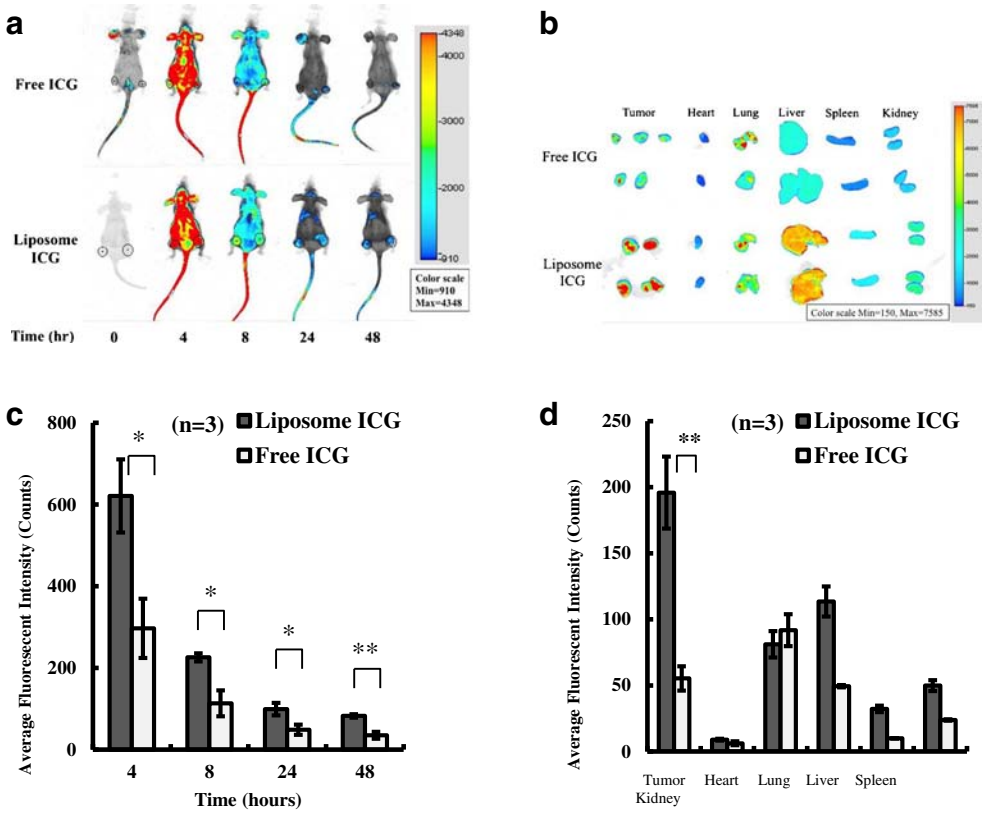

Fig. 4 (**a**) NIR fluorescence imaging of athymic nude mice with established MDA-MB-468 xenograft model, using the 800 nm spectral channel. Mice were imaged at 0, 4, 8, 24, and 48 h following i.v. dosing of 5 mg/kg FRICG or LPICG. One representative mouse is shown out of the three scanned mice per group with ellipses indicating the tumor location on both flanks. (**b**) Terminal biodistribution assessment to evaluate the tumors, heart, lungs, liver, spleen, and kidneys imaged 24 h after dosing with FRICG or LPICG. (**c**) Average fluorescent intensity signal counts of tumors located on flanks of nude mice imaged 4, 8, 24, and 48 h after dosing with 5 mg/kg FRICG or LPICG. Representative values are the mean fluorescence counts ± SD ($n = 3$). (**d**) Average fluorescent intensity in organs dissected 24 h after dosing with 5 mg/kg FRICG or LPICG. Plotted values correspond to mean fluorescence intensity counts ± SD ($n = 3$). Statistical significance is indicated by $p < 0.05$ (*) and < 0.01 (**).

in vivo efficacy (28). Based on doses of ICG in the literature as well as a small-scale pilot study, a single dose of 5 mg/kg FRICG or LPICG was selected to determine the anti-tumor effects of PDT over 54 days. After establishing the size of the tumor, mice were injected with PBS, FRICG or LPICG on day 9, and those in laser treatment groups were irradiated 6 h post-injection.

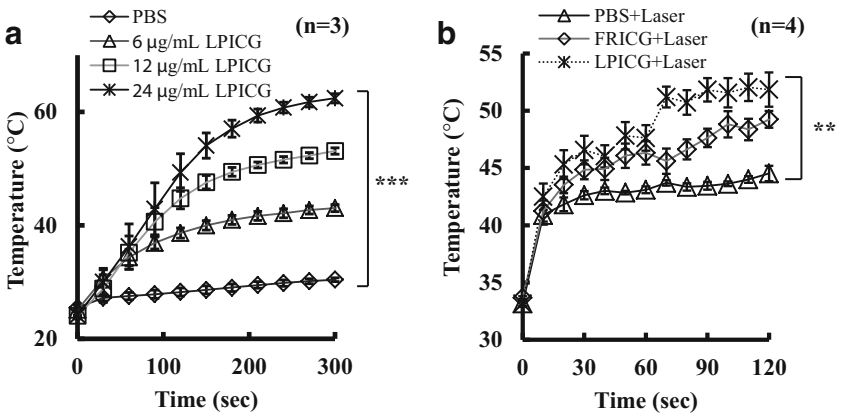

Fig. 5 (**a**) *In vitro* temperature elevation of aqueous solutions containing LPICG with various encapsulated ICG concentrations during a 5-min NIR irradiation (808 nm, 2 W). Results are the mean values ± SD ($n = 3$). (**b**) *In vivo* tumor surface temperature changes during a 2-min NIR irradiation (808 nm, 2 W), 6 h after i.v. dosing of PBS, or 5 mg/kg FRICG or LPICG. Plotted values represent the mean temperature ± SD ($n = 4$). Student *t*-test was performed to evaluate the statistical significance between groups for both *in vitro* and *in vivo* with *p* values < 0.01 (**) and < 0.001 (***).

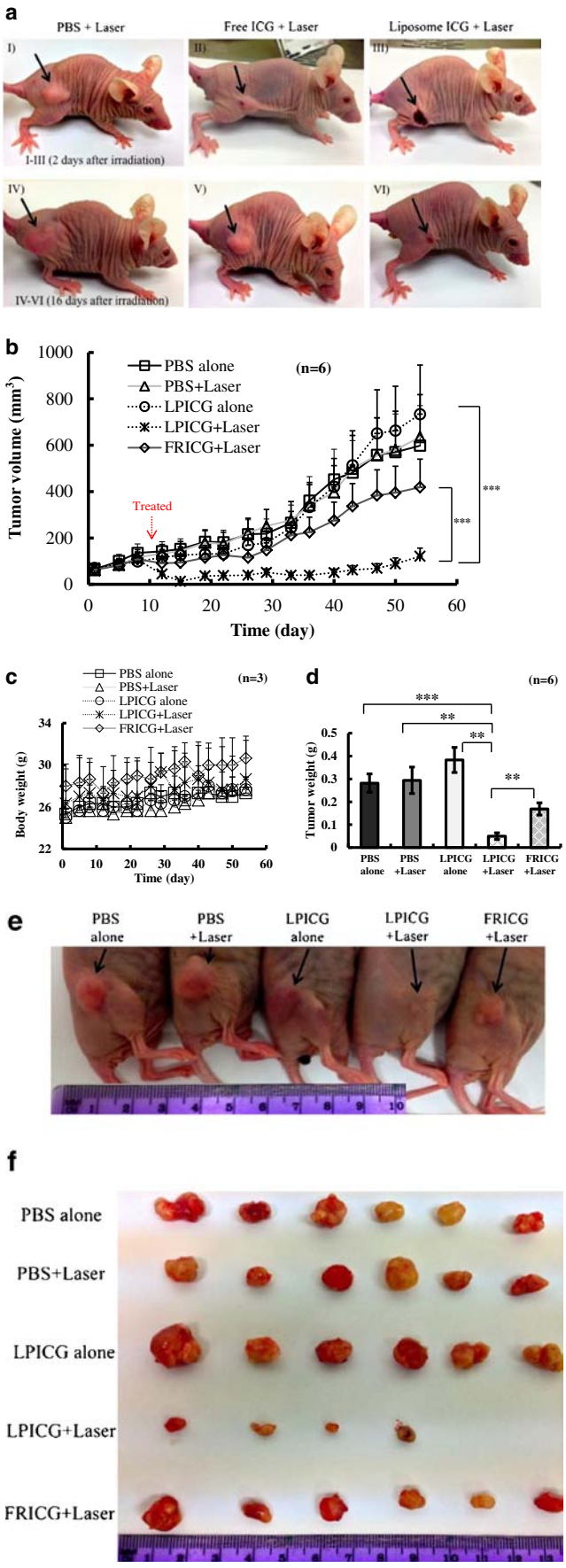

Fig. 6 *In vivo* PDT of MDA-MB-468 xenograft model established in nude mice using NIR light emitting at 808 nm and 2 W/cm^2 energy for 2 min, 6 h post i.v. administration. (**a**) Mice were injected with PBS (I, IV), 5 mg/kg FRICG (II, V), or 5 mg/kg LPICG (III, VI). PBS plus laser control group illustrates negligible damage to the tumor, while FRICG shows minimal damage and LPICGC exhibits significant damage to the tumor 2 days after illumination. (**b**) Evaluation of PDT anti-tumor efficacy over 54 days in tumor-bearing mice treated with PBS alone, PBS plus laser, LPICG alone, LPICG plus laser, and FRICG plus laser. NIR irradiation was initiated on the 9th day for the designated groups and was performed 6 h after dosing for 2 min emitting at 808 nm and 2 W/cm^2 fluence level. Plotted values are representative of mean tumor volumes ± SD ($n = 6$). (**c**) Total body weight of tumor-bearing mice throughout the course of treatment to demonstrate tolerability. Values are representative of the mean weight ± SD ($n = 3$). (**d**) Depiction of weighed excised tumors from each treatment and control group. Plotted values are representative of the mean weight ± SD ($n = 6$), with statistical significance denoted as $p < 0.01$ (**) and < 0.001 (***). (**e**) Representative images of tumor mass growth on the final day of study before excision. (**f**) Excised tumors from each group indicating significant proliferation of the tumor mass for control groups with considerably smaller volumes for PDT treatment groups and even partial eradication for LPICG-PDT group.

Tumor growth progression was monitored every 3–4 days. As demonstrated in Fig. 6a, mice that were administered with PBS or FRICG and treated with 808 nm laser irradiation at 2 W/cm^2 for 2 min showed negligible and minor subsequent damage to the tumor and increasing proliferation of the mass after 16 days. In contrast, mice dosed with LPICG followed by irradiation using the same conditions exhibited significant and immediate damage to the tumor site with nearly complete eradication of the mass after 16 days. The drastic and significant difference in tumor nodule growth observed between LPICG-PDT treatment group and control groups over the course of 54 days is illustrated in Fig. 6b. Mice administered with LPICG and treated with laser irradiation were found to have the most drastic effect on tumor growth retardation, which was statistically significant compared to FRICG and PBS control groups with $p < 0.001$ and < 0.01, respectively. Furthermore, the irradiated mice demonstrated very high treatment tolerability as presented by minor fluctuations in total body mass compared to the non-irradiated control groups throughout the study (Fig. 6c). At the terminal time-point, drastic differences in actual size of excised tumors were observed between treatment and control groups with significantly smaller volumes for LPICG-PDT *versus* FRICG-PDT (Fig. 6d; $p < 0.01$). Moreover, the tumor masses were found to be much smaller for the liposomal PDT group compared to PBS, PBS plus laser, and LPICG alone control groups with $p < 0.001$, < 0.01, and < 0.01, respectively (Fig. 6d). A representative mouse from each subgroup is also shown in Fig. 6e with clearly marked tumor regions to visually demonstrate the differences in tumor growth. As illustrated by the image, the tumors on the mouse from LPICG-PDT treatment group appear to have been completely eradicated. Additionally, all tumor masses were excised at the completion of anti-tumor efficacy study on day 54 and imaged (Fig. 6f). As depicted in the figure, two out of six original tumors

in the LPICG-PDT treatment group were completely eradicated with the remaining four tumors drastically reduced in size as compared to other groups.

Thus, the results from this study exhibited positive and promising outcomes regarding the application of LPICG-PDT for localized and effective treatment of TNBC, while minimizing unwanted side effects and toxicities. Moreover, with the increasing attention gained by NIR dyes in medical imaging applications, the encapsulation of ICG in liposomes offers great potential for image-guided delivery and real-time biodistribution monitoring as demonstrated in our study. Hence, this study contributed to developing and characterizing a targeted and theranostic-based liposomal formulation capable of achieving both pharmacological effects and real-time formulation monitoring.

CONCLUSIONS

It was observed that selective and localized PDT can achieve tumor destruction *in vivo,* while preventing damage to non-tumorous tissue as demonstrated in a TNBC xenograft murine model. In summary, we demonstrated the potential of using LPICG to improve the anti-tumor therapeutic efficacy of PDT in tumor-bearing mice, with excellent tolerability and possible tumor eradication. Our experiments confirmed that significant cytotoxicity is obtained *in vitro* when LPICG is stimulated by 808 nm laser light. Furthermore, we demonstrated the pharmacokinetic enhancement of ICG *via* using a liposome-based delivery approach. Additionally, it was shown that irradiation of the liposomal formulation can induce elevation of temperature both *in vitro* and *in vivo*, which may in turn hold potential in achieving photothermal-mediated cytotoxic effects. Lastly, NIR fluorescence imaging and biodistribution assessment exhibited enhanced tumor accumulation using LPICG. Taken together these results provide valuable insights into using nanocarrier-based photosensitizers such as LPICG for improved anti-tumor PDT efficacy as well as simultaneous real-time imaging.

ACKNOWLEDGMENTS AND DISCLOSURES

We thank Dr. LaTonia Taliaferro-Smith and Tongrui Liu of the Winship Cancer Institute of Emory University for their donation of MDA-MB-468. We would also like to thank Dr. Ajay Banga of the Transdermal Delivery Laboratory at Mercer University for donation of pig ear skin tissues. We would like to acknowledge Dr. Ayyappa Chaturvedula and Vineet Goti from the Department of Pharmacy Practice at Mercer University for their valuable contributions to interpretation of pharmacokinetic analysis. This work was funded in part by the Georgia Cancer Coalition's Cancer Research Award.

REFERENCES

1. Dolmans DE, Fukumura D, Jain RK. Photodynamic therapy for cancer. Nat Rev Cancer. 2003;3(5):380–7.
2. Triesscheijn M, Baas P, Schellens JH, Stewart FA. Photodynamic therapy in oncology. Oncologist. 2006;11(9):1034–44.
3. Allison RR, Bagnato VS, Sibata CH. Future of oncologic photodynamic therapy. Future Oncol. 2010;6(6):929–40.
4. Agostinis P, Berg K, Cengel KA, Foster TH, Girotti AW, Gollnick SO, *et al.* Photodynamic therapy of cancer: an update. CA Cancer J Clin. 2011;61(4):250–81.
5. Allison RR, Mota HC, Bagnato VS, Sibata CH. Bio-nanotechnology and photodynamic therapy–state of the art review. Photodiagnosis Photodyn Ther. 2008;5(1):19–28.
6. Huang Z. A review of progress in clinical photodynamic therapy. Technol Cancer Res Treat. 2005;4(3):283–93.
7. Lee SJ, Koo H, Jeong H, Huh MS, Choi Y, Jeong SY, *et al.* Comparative study of photosensitizer loaded and conjugated glycol chitosan nanoparticles for cancer therapy. J Control Release. 2011;152(1):21–9.
8. Huang P, Li Z, Lin J, Yang D, Gao G, Xu C, *et al.* Photosensitizer-conjugated magnetic nanoparticles for in vivo simultaneous magnetofluorescent imaging and targeting therapy. Biomaterials. 2011;32(13):3447–58.
9. Lee SJ, Koo H, Lee D-E, Min S, Lee S, Chen X, *et al.* Tumor-homing photosensitizer-conjugated glycol chitosan nanoparticles for synchronous photodynamic imaging and therapy based on cellular on/off system. Biomaterials. 2011;32(16):4021–9.
10. Jeong H, Huh M, Lee SJ, Koo H, Kwon IC, Jeong SY, *et al.* Photosensitizer-conjugated human serum albumin nanoparticles for effective photodynamic therapy. Theranostics. 2011;1:230–9.
11. Tian J, Ding L, Xu HJ, Shen Z, Ju H, Jia L, *et al.* Cell-specific and pH-activatable rubyrin-loaded nanoparticles for highly selective near-infrared photodynamic therapy against cancer. J Am Chem Soc. 2013;135(50):18850–8.
12. Gamal-Eldeen AM, El-Daly SM, Borai IH, Wafay HA, Abdel-Ghaffar AR. Photodynamic therapeutic effect of indocyanine green entrapped in polymeric nanoparticles and their anti-EGFR-conjugate in skin cancer in CD1 mice. Photodiagnosis Photodyn Ther. 2013;10(4):446–59.
13. Zhang Y, Qian J, Wang D, Wang Y, He S. Multifunctional gold nanorods with ultrahigh stability and tunability for in vivo fluorescence imaging, SERS detection, and photodynamic therapy. Angew Chem Int Ed Engl. 2013;52(4):1148–51.
14. Ding H, Sumer BD, Kessinger CW, Dong Y, Huang G, Boothman DA, *et al.* Nanoscopic micelle delivery improves the photophysical properties and efficacy of photodynamic therapy of protoporphyrin IX. J Control Release. 2011;151(3):271–7.
15. Schaafsma BE, Mieog JS, Hutteman M, van der Vorst JR, Kuppen PJ, Löwik CW, *et al.* The clinical use of indocyanine green as a near-infrared fluorescent contrast agent for image-guided oncologic surgery. J Surg Oncol. 2011;104(3):323–32.
16. Taichman GC, Hendry PJ, Keon WJ. The use of cardio-green for intraoperative visualization of the coronary circulation: evaluation of myocardial toxicity. Tex Heart Inst J. 1987;14(2):133–8.
17. Yuan A, Wu J, Tang X, Zhao L, Xu F, Hu Y. Application of near-infrared dyes for tumor imaging, photothermal, and photodynamic therapies. J Pharm Sci. 2013;102(1):6–28.
18. Frangioni JV. In vivo near-infrared fluorescence imaging. Curr Opin Chem Biol. 2003;7(5):626–34.
19. Mordon S, Devoisselle JM, Soulie-Begu S, Desmettre T. Indocyanine green: physicochemical factors affecting its fluorescence in vivo. Microvasc Res. 1998;55(2):146–52.
20. Desmettre T, Devoisselle J, Mordon S. Fluorescence properties and metabolic features of indocyanine Green (ICG) as related to angiography. Surv Ophthalmol. 2000;45(1):15–27.

21. Derycke A. Liposomes for photodynamic therapy. Adv Drug Deliv Rev. 2004;56(1):17–30.
22. Paszko E, Ehrhardt C, Senge MO, Kelleher DP, Reynolds JV. Nanodrug applications in photodynamic therapy. Photodiagnosis Photodyn Ther. 2011;8(1):14–29.
23. Chatterjee DK, Fong LS, Zhang Y. Nanoparticles in photodynamic therapy: an emerging paradigm. Adv Drug Deliv Rev. 2008;60(15): 1627–37.
24. Chen B, Pogue BW, Hasan T. Liposomal delivery of photosensitising agents. Expert Opin Drug Deliv. 2005;2(3):477–87.
25. Maeda H, Wu J, Sawa T, Matsumura Y, Hori K. Tumor vascular permeability and the EPR effect in macromolecular therapeutics: a review. J Control Release. 2000;65(1–2):271–84.
26. Klibanov AL, Maruyama K, Torchilin VP, Huang L. Amphipathic polyethyleneglycols effectively prolong the circulation time of liposomes. FEBS Lett. 1990;268(1):235–7.
27. Turner DC, Moshkelani D, Shemesh CS, Luc D, Zhang H. Near-infrared image-guided delivery and controlled release using optimized thermosensitive liposomes. Pharm Res. 2012;29(8):2092–103.
28. Shemesh CS, Hardy CW, Yu DS, Fernandez B, Zhang H. Indocyanine green loaded liposome nanocarriers for photodynamic therapy using human triple negative breast cancer cells. Photodiagnosis Photodyn Ther. 2014;11(2):193–203.
29. De Ruijter TC, Veeck J, de Hoon JP, van Engeland M, Tjan-Heijnen VC. Characteristics of triple-negative breast cancer. J Cancer Res Clin Oncol. 2011;137(2):183–92.
30. Alli E, Sharma VB, Sunderesakumar P, Ford JM. Defective repair of oxidative dna damage in triple-negative breast cancer confers sensitivity to inhibition of poly(ADP-ribose) polymerase. Cancer Res. 2009;69(8):3589–96.
31. Montazerabadi AR, Sazgarnia A, Bahreyni-Toosi MH, Ahmadi A, Aledavood A. The effects of combined treatment with ionizing radiation and indocyanine green-mediated photodynamic therapy on breast cancer cells. J Photochem Photobiol B. 2012;109:42–9.
32. Lim HJ, Oh CH. Indocyanine green-based photodynamic therapy with 785 nm light emitting diode for oral squamous cancer cells. Photodiagnosis Photodyn Ther. 2011;8(4):337–42.
33. Abels C, Fickweiler S, Weiderer P, Bäumler W, Hofstädter F, Landthaler M, *et al.* Indocyanine green (ICG) and laser irradiation induce photooxidation. Arch Dermatol Res. 2000;292(8):404–11.
34. Henderson BW, Dougherty TJ. How does photodynamic therapy work? Photochem Photobiol. 1992;55(1):145–57.
35. Guelluy PH, Fontaine-Aupart MP, Grammenos A, Lécart S, Piette J, Hoebeke M. Optimizing photodynamic therapy by liposomal formulation of the photosensitizer pyropheophorbide-a methyl ester: in vitro and ex vivo comparative biophysical investigations in a colon carcinoma cell line. Photochem Photobiol Sci. 2010;9(9):1252–60.
36. Wang J, Sui M, Fan W. Nanoparticles for tumor targeted therapies and their pharmacokinetics. Curr Drug Metab. 2010;11(2):129–41.
37. Saxena V, Sadoqi M, Shao J. Polymeric nanoparticulate delivery system for Indocyanine green: biodistribution in healthy mice. Int J Pharm. 2006;308(1–2):200–4.
38. Khurana M, Ulrich S, Kim A, Moriyama Y, Netchev G, Akens MK, *et al.* Biodistribution and pharmacokinetic studies of a porphyrin dimer photosensitizer (Oxdime) by fluorescence imaging and spectroscopy in mice bearing xenograft tumors. Photochem Photobiol. 2012;88(6):1531–8.
39. Zheng X, Xing D, Zhou F, Wu B, Chen WR. Indocyanine green-containing nanostructure as near infrared dual-functional targeting probes for optical imaging and photothermal therapy. Mol Pharm. 2011;8(2):447–56.
40. Chen WR, Adams RL, Higgins AK, Bartels KE, Nordquist RE. Photothermal effects on murine mammary tumors using indocyanine green and an 808-nm diode laser: an in vivo efficacy study. Cancer Lett. 1996;98(2):169–73.
41. Suganami A, Toyota T, Okazaki S, Saito K, Miyamoto K, Akutsu Y, *et al.* Preparation and characterization of phospholipid-conjugated indocyanine green as a near-infrared probe. Bioorg Med Chem Lett. 2012;22(24):7481–5.
42. Shafirstein G, Bäumler W, Hennings LJ, Siegel ER, Friedman R, Moreno MA, *et al.* Indocyanine green enhanced near-infrared laser treatment of murine mammary carcinoma. Int J Cancer. 2012;130(5):1208–15.